

Comparison of characteristic and Gutenberg–Richter models for time-dependent $M \geq 7.9$ earthquake probability in the Nankai-Tokai subduction zone, Japan

Tom Parsons,¹ Rodolfo Console,² Giuseppe Falcone,² Maura Murru² and Ken'ichiro Yamashina³

¹U.S. Geological Survey, MS-999, 345 Middlefield Rd. Menlo Park, CA 94025, USA

²Istituto Nazionale di Geofisica e Vulcanologia (INGV), Via di Vigna Murata 605, 00143 Roma, Italy. E-mail: maura.murru@ingv.it

³Earthquake Research Institute (ERI), University of Tokyo, Yayoi 1-1-1, Bunkyo-ku, Tokyo 113-0032, Japan

Accepted 2012 June 27. Received 2012 June 27; in original form 2011 November 29

SUMMARY

Earthquake forecasts are usually underinformed, and can be plagued by uncertainty in terms of the most appropriate model, and parameter values used in that model. In this paper, we explore the application of two different models to the same seismogenic area. The first is a renewal model based on the characteristic earthquake hypothesis that uses historical/palaeoseismic recurrence times, and fixed rupture geometries. The hazard rate is modified by the Coulomb static stress change caused by nearby earthquakes that occurred since the latest characteristic earthquake. The second model is a very simple earthquake simulator based on plate-motion, or fault-slip rates and adoption of a Gutenberg–Richter magnitude–frequency distribution. This information is commonly available even if historical and palaeoseismic recurrence data are lacking. The intention is to develop and assess a simulator that has a very limited parameter set that could be used to calculate earthquake rates in settings that are not as rich with observations of large-earthquake recurrence behaviour as the Nankai trough. We find that the use of convergence rate as a primary constraint allows the simulator to replicate much of the spatial distribution of observed segmented rupture rates along the Nankai, Tonankai and Tokai subduction zones. Although we note rate differences between the two forecast methods in the Tokai zone, we also see enough similarities between simulations and observations to suggest that very simple earthquake rupture simulations based on empirical data and fundamental earthquake laws could be useful forecast tools in information-poor settings.

Key words: Time series analysis; Spatial analysis; Probability distributions; Seismic cycle; Earthquake interaction, forecasting, and prediction; Statistical seismology.

1 INTRODUCTION

Is it best to calculate seismic hazard by attempting to identify every possible fault segment and their characteristic earthquake ruptures and rate cycles? The answer is probably yes when there is enough information to do so. Unfortunately, in most places seismic hazard calculations are underinformed. Here, we compare techniques of characteristic segmentation with the use of a simple earthquake simulator based on empirical observations that are typically available in most settings: (1) long term average fault-slip rates, and (2) the slope (b -value) of the earthquake catalogue magnitude–frequency distribution. We apply both techniques at one of Earth's best-identified set of fault segments, the Nankai, Tonankai and Tokai subduction zones in southwest Japan (Fig. 1), focusing on comparative probabilistic forecasting on the Tokai segment. The idea is that if a simple Gutenberg–Richter model can adequately explain a data-rich setting

within uncertainties, then it can be used in data-poor settings as a reasonable default method for seismic hazard calculations.

A combination of historic earthquake, palaeoearthquake and tsunami records has enabled the development of a lengthy (AD684–AD1946) catalogue of large ($M \geq 7.9$) earthquakes that appear to have occurred repeatedly within the same spatial zones or segments, sometimes rupturing adjacent zones as doublets, or rupturing across the entire ~650-km-long Nankai-Tokai zone (Ando 1975b; Ishibashi & Satake 1998). Being perhaps the primary example of a geometrically segmented subduction margin, the Nankai-Tokai zone is an ideal place to compare a simple earthquake simulator that does not constrain earthquakes to occur on defined segments with methods that do rely on segmentation.

In this paper, we first apply a well-known methodology (Shimazaki & Nakata 1980; Working Group on California Earthquake Probabilities (WGCEP) 1995, 2003, 2008; Stein *et al.* 1997;

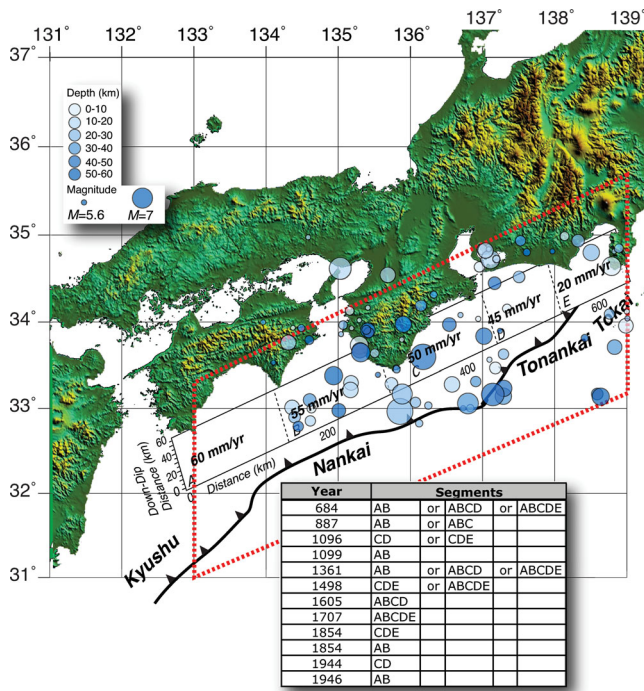


Figure 1. Location of the Kyushu, Nankai, Tonankai and Tokai subduction zones in Japan. The bathymetric trace of the base of the steep inner slope along the Nankai trough is shown. Segments labelled A–E (Ando 1975b) and past earthquake rupture locations are defined by Ishibashi & Satake (1998) and slip rates are given by Mitsui & Hirahara (2004). $M \geq 5.6$ earthquakes [source: Japan Meteorological Agency (JMA)] that occurred in the region between 1926 and 2010 are shown shaded by depth (maximum depth is 60 km). Red dashed box outlines seismicity search area; $M \geq 5.7$ events were used in the magnitude–frequency plot of Fig. 5.

Matthews *et al.* 2002) to the assessment of the occurrence probability of future earthquakes on the subduction zone along the southern coast of Japan, conditional to the time elapsed since the last characteristic earthquake on each fault and to the history of the following events on the neighbouring active sources. The application is done on the north easternmost segment of the Nankai–Tokai subduction zone, known as the Tokai segment and labelled with E in Fig. 1. The Tokai segment last ruptured in 1854, and before that in 1707 and 1498. All of these events were great earthquakes of magnitude 8.4 or larger. They ruptured also the other segments from A to D, but unlike these four segments, the Tokai segment did not break during the more recent events in 1944 (C–D) and 1946 (A–B). These facts were noted in the 1970s by Ando (1975a) and Ishibashi (1976, 1980, 1981). Since then, much effort was devoted to studying historic earthquakes and the tectonic structure of the Tokai area. In 1978, the Japanese legislature adopted the Large-Scale Earthquake Countermeasures Act with the sole target of the Tokai earthquake. In 1979, the Tokai segment was declared an ‘area under intensified measures against earthquake disaster’. As a consequence, widespread, persistent public education raised awareness about the expected effects of the next Tokai earthquake, which became a popular subject of concern (Mogi 2004). We start from the estimate of the probability of occurrence in the next 10 and 30 yr for a characteristic earthquake on the Tokai segment, based on a renewal model. The occurrence rate of the characteristic earthquake is calculated taking into account also the permanent perturbation because of the Coulomb stress change (ΔCFF) caused by slip on the neighbouring faults after the occurrence of the latest event. The results show that

the estimated effect of earthquake interaction in this region is small if compared with the uncertainties affecting the statistical model used for the basic time-dependent hazard assessment.

In the following sections of the paper, we approach the same problem by simulating the long-term earthquake distribution on a set of segments. We apply the simulator to a simplified model of the Nankai, Tonankai and Tokai zones using the plate convergence rates and a Gutenberg–Richter magnitude–frequency distribution as primary data inputs. From 100 simulations, we develop a set of synthetic earthquake ruptures that we compare with the observed record. Finally, we demonstrate how the synthetic rupture record might be used to make earthquake recurrence inferences and probability calculations.

Our simplifying choices with regard to modelling earthquake rates takes us into the debate whether great earthquakes are constrained to occur as characteristic ruptures, a model that assumes fault segmentation, near-total stress reduction and quasi-periodic recurrence. Of these assumptions, we focus primarily on the segmentation question and implied spatial distribution of great earthquakes and their magnitudes.

2 THE HISTORICAL EARTHQUAKE CATALOGUE

Despite the wealth of historical information that characterizes the seismicity of the Nankai–Tokai trough, a definitive list of repeating earthquakes on the five main segments recognized with the letters A to E on this seismogenic structure (Fig. 1) is not yet fully agreed upon. The historical earthquake evidence was examined and reported by the Subcommittee for Long-Term Evaluation, Earthquake Research Committee (ERC 2001). According to the ERC (2001) report, the most reliable dates of great Nankai and/or Tonankai earthquakes before AD1498 were November 29 AD684, August 26 AD887, December 17 AD1096, November 22 AD1360 and August 3 AD1361, with some concern about the November 22 AD1360 event. Ishibashi & Satake (1998) cast doubt that the November 22 AD1360 event was a characteristic earthquake in the Tonankai (or Tokai) segment, and suggested that an event around August 1 AD1361 might be one of a pair with the AD1361 Nankai earthquake. We leave this hypothesis as an alternative option.

Sykes & Menke (2006) note that the mean recurrence time of characteristic earthquakes as reported in the list accepted by the ERC (2001) report before AD1361 is much larger than that computed from the events occurred after that year. They use this circumstance to infer that some old earthquakes are missing in that list. They justify the lack of historical information by the great civil unrest that characterized the history of Japan in the centuries before AD1361. Sykes & Menke (2006) quote the work done by Sangawa (1999), who discusses archeologically determined dates for two potential characteristic earthquakes that might have occurred in AD999 and AD1233. These two events, added to the previously acknowledged list, fill large temporal gaps and yield a sequence characterized by much more regular behaviour and smaller coefficient of variation. However, a more recent study published by Sangawa (2011) doesn’t include any archaeological information about an earthquake between AD887 and AD1099.

The hypothesis of the two archaeological events of AD999 and AD1233 to be retained as characteristic earthquakes of the Nankai segment is not yet fully accepted by the Japanese seismological community. Mochizuki & Obana (2003) remarked that there are difficulties in discerning whether these events were plate-boundary

or intraplate earthquakes. Further, Ishibashi (1999) questioned the evidence for possible events suggested to have happened during the 262-yr interval between the AD1096–1099 earthquakes and the AD1361 earthquake. He concluded that the question of whether an interevent time of about 200 yr is appropriate for the earthquakes before AD1361 has not yet been answered.

We adopted the list of 12 earthquakes presented in the inset table of Fig. 1, with its various additional options, in view of the common understanding diffused in the Japanese seismological community. Making this choice, we accept the fact that the present result is not conclusive but assumed it as a working hypothesis, subject to revision based on the collection of a more complete list of earthquakes.

3 APPLICATION OF A TIME-PREDICTABLE MODEL FOR EARTHQUAKE OCCURRENCE PROBABILITY

3.1 Statistical analysis based on the Brownian Passage Time (BPT) distribution

A simple spring-mass model proposed by Reid (1910) in his pioneering work, has been the most popular idea adopted so far for modelling earthquake occurrence. This idea led to the development of the concepts of seismic gap (Mogi 1968), and the characteristic earthquake (Schwartz & Coppersmith 1984; Nishenko & Buland 1987; Wesnousky 1994), where earthquakes recur quasi-periodically on identified fault segments. In this context, fault segmentation of the Nankai-Tokai trough zone was introduced, and became very popular at least since the 1970s with a number of studies published by Japanese scientists (see e.g. Ando 1975a; Rikitake 1976; Utsu 1977; Ishibashi 1981). At the same time, the same Japanese scientists have preferably applied the Weibull probability density distribution (PDF) to the recurrence times of the Tokai earthquake (Hagiwara 1974; Rikitake 1975, 1977).

In this application we assume that the Tokai earthquake interevent time is modelled by the BPT (inverse Gaussian) PDF (Kagan & Knopoff 1987; Matthews *et al.* 2002). The recurrence time T_r and the coefficient of variation (aperiodicity) α parameters of this distribution for $M = 8$ earthquakes on the Tokai segment of the Nankai-Tokai fault zone are easily computed from the occurrence times reported in the inset table of Fig. 1, assuming that this segment (E) has ruptured six times after and including the event of AD684 (see e.g. Console *et al.* 2008):

$$T_r = 234.0 \text{ yr}; \alpha = 0.428.$$

Here the recurrence time and its standard deviation are obtained directly as the average and the standard deviation of the five interevent times. Monte Carlo analysis (Parsons 2008) on the maximum interpreted number of Tokai ruptures (6) yields the exact same mean of $T_r = 234$ yr, but with a slightly different coefficient of variation of $\alpha = 0.5$ for a BPT distribution. We call this assumption a maximum rate interpretation.

For any time interval of 10 yr, the probability of occurrence according to a Poisson time-independent model of characteristic earthquake on the Tokai fault is 0.042 (4.2 per cent); the 30-yr probability is 12.0 per cent. Application of the BPT density distribution to the computation of the conditional probability of occurrence of this characteristic earthquake for the next 10 yr after 2012 January 1 (given an elapsed time of 157 yr after the latest characteristic earthquake) leads to an estimate of 6.1 per cent for such probability; the 30-yr probability is 18.7 per cent.

To assess the impact that a different assumption about the history of past events on the Tokai fault has on the seismic hazard estimate, we consider as an alternative hypothesis also that the Tokai segment has ruptured only three times after AD684, that is, in AD1498, 1707 and 1854. We call this assumption a minimum rate interpretation. Repeating the computations, we obtain in this case an interevent time $T_r = 390$ yr, a Poisson time-independent probability of 2.5 per cent for a new event in the next 10 yr, a coefficient of variation $\alpha = 0.771$ and a conditional probability of 3.0 per cent for the BPT distribution. The 30-yr time-independent probability is 7.4 per cent and that for the time-dependent model is 9.0 per cent.

Another approach to compute the recurrence time for an earthquake sequence is dividing the total observation time by the number of events. In this case, the time following the latest event until the present is included in the total observation time. This approach is convenient when the record includes an open interval (i.e. a time interval preceding the oldest event during which we know that no events occurred), which is also included in the total observation time. This open interval may be subjective, depending on our judgment about the non-occurrence of events in a period of time characterized by scarce information. For the series 1498 A.D., 1707 A.D. and 1854 A.D., considering only the period from 1498 A.D. up to the present as observation time, we obtain a recurrence time of 171 yr. For the same series of three events, including the information that no events have occurred between 684 A.D. and 1498 A.D., we obtain a recurrence time of 442 yr. In principle, the open interval could extend even before 684 A.D., with the consequence of increasing both the interevent time and the coefficient of variation. For sake of comparison, we have also carried out the same statistical analysis on the Nankai (A–B) and Tonankai (C–D) fault segments. For each of these segments we have made two different assumptions, obtaining the following results as of 2012 January:

(1) Nankai segment (minimum rate), eight events after and including AD684; $T_r = 180.3$ yr, $\alpha = 0.346$; Poisson probability for 10 yr = 5.4 per cent, conditional probability for 10 yr = 0.50 per cent; Poisson probability for 30 yr = 15.3 per cent, conditional probability for 30 yr = 3.9 per cent;

(2) Nankai segment (maximum rate), nine events after and including AD684; $T_r = 157.8$ yr, $\alpha = 0.364$; Poisson probability for 10 yr = 6.1 per cent; conditional probability for 10 yr = 1.9 per cent; Poisson probability for 30 yr = 17.3 per cent, conditional probability for 30 yr = 9.7 per cent;

(3) Tonankai segment (minimum rate), seven events after and including AD684; $T_r = 210.0$ yr, $\alpha = 0.669$; Poisson probability for 10 yr = 4.7 per cent, conditional probability for 10 yr = 3.7 per cent; Poisson probability for 30 yr = 13.3 per cent, conditional probability for 30 yr = 12.5 per cent;

(4) Tonankai segment (maximum rate), eight events after and including AD684; $T_r = 180.0$ yr, $\alpha = 0.607$; Poisson probability for 10 yr = 5.4 per cent, conditional probability for 10 yr = 4.6 per cent; Poisson probability for 30 yr = 15.3 per cent, conditional probability for 30 yr = 15.5 per cent.

This analysis shows that for the Nankai and Tonankai segments, the conditional probability of the next event is smaller than that found for the Tokai segment under the maximum rate interpretation, even if the time-independent Poisson probability is larger. The conditional probability in these two segments is also smaller under the time-dependent hypothesis than under a time-independent Poisson model. This is especially true for the Nankai segment because the coefficient of variation α is smaller than that found for the Tonankai segment. Compare, for instance, cases 1 and 4, for which

Table 1. Geometrical parameters of fault segments ruptured by characteristic earthquakes in the Tokai fault.

Date	Magnitude M	Fault length L (km)	Fault width W (km)	$(LW)^{1/2}$ (km)	Max. slip Δu_{\max} (m)	Stress drop $\Delta\sigma$ (MPa)
1361 August 3	–	–	–	–	–	–
1498 July 9	8.6	220	80	132	8.00	3.6
1707 October 28	8.4	230	70	127	8.00	3.8
1854 December 23	8.4	115	70	90	4.00	2.7

the recurrence time, and consequently the Poisson probability, are almost identical.

It may be interesting to note that the official forecasts given by the Headquarters for Earthquake Research Promotion assign higher values to the probabilities of occurrence of a characteristic earthquake to both the Nankai and Tonankai segments. The respective values are of the order of 60 per cent and 70 per cent. They are based on the concept of the time-predictable model, assuming an α -value equal to 0.20, and the fact that the latest large earthquakes in 1946 and 1944 were relatively small in size considering the amount of crustal deformation, tsunami magnitude and distribution of seismic intensities. Taking into account these circumstances, the recurrence times computed as 114.0 yr for the Nankai segment and 111.6 yr for the Tonankai segment are shortened to 86.4 yr and 90.1 yr, respectively.

As for the Nankai and the Tonankai segments, the probability assigned by the official forecasts of the Headquarters for Earthquake research Promotion for the Tokai segment is higher than ours. In fact, their forecast, assuming the occurrence of four characteristic events (including AD1605) during the period 1498–1854, with a recurrence time of 118.8 yr and $\alpha = 0.20$ (just the same as that for the Tonankai segment), is of 88 per cent probability for the next 30 yr.

3.2 Effect of stress interaction between faults

In real circumstances earthquake sources may interact, causing probability gains or losses with respect to what is expected by a simple renewal model. To assess the influence of fault interaction on these estimates, we apply the methodology described by Console *et al.* (2008, 2010). We first need to compute the annual stressing rate caused by tectonic loading on the Tokai earthquake source. To do so, we assume that the cumulative stress built up by tectonic loading is entirely released by characteristic earthquakes. The parameters of these earthquakes are known back to the earthquake of 1498 July 9 (Sato *et al.* 1989), and are listed in Table 1.

Note that the geometrical parameters refer to the part of the fault containing the Tokai segment, which is modelled as a unique rectangular source. However, the given magnitudes refer to all the segments that broke during earthquakes in which the Tokai segment participated.

Stress-drop values ($\Delta\sigma$) were computed through an approximate relation introduced by Console & Catali (2007), and denoted consistent values around an average of 3.4 MPa. The total stress released by the three earthquakes was 10.1 MPa. Under the maximum rate interpretation, the Tokai segment has released the accumulated tectonic stress in 1361, dividing the total stress by the time interval between 1854–1361 (493 yr), we obtain a stressing rate $\dot{\tau} = 0.020$ MPa yr⁻¹. Note that Table 1 reports the values of the maximum coseismic slip for each event on the fault. So, dividing the total slip (20 m) by 493 yr, and assuming the approximate relation $\overline{\Delta u} = \frac{\pi^2}{16} \Delta u_{\max}$ between the average and the maximum slip on a

rectangular fault (Console & Catali 2007) we obtain an average slip rate of 25 mm yr⁻¹, a little higher than the 20 mm yr⁻¹ value reported by Mitsui & Hirahara (2004). However, under a minimum rate interpretation, we consider that the same total stress was accumulated between 1854–684 (1170 yr), and we obtain a much smaller slip rate of 10.5 mm yr⁻¹. This value could be considered as a sort of lower bound estimate, obtained neglecting the contribution of the stress-drop released by smaller earthquakes on the same fault segment.

We computed the ΔCFF from large and moderate earthquakes that occurred close to or with epicentres just inside the horizontal projection of the Tokai segment (E, Fig. 1) after the latest Ansei-Tokai earthquake, which occurred on 1854 December 23. The source parameters of all the causative earthquakes before 1987 were taken from Sato *et al.* (1989). Other source parameters were resumed from more recent technical reports.

ΔCFF is computed by resolving the stress tensor on the focal mechanism of the target source. In the computation we assumed a coefficient of friction $\mu = 0.4$. It is well-known that the coefficient of friction on a real fault is a parameter affected by large uncertainty. However, a numerical test carried out assuming $\mu = 0.0$ (no friction at all) has shown little variations in the results. The target event parameters were adopted from those reported by Sato *et al.* (1989) for the Tokai segment of the 1854 earthquake, characterized by linear dimensions $L = 115$ km, $W = 70$ km and focal mechanism $\phi = 198^\circ$, $\delta = 34^\circ$, $\lambda = 71^\circ$. Fig. 2 shows the map of ΔCFF for this specific area, computed at a constant depth of 20 km. This map was obtained from the values of ΔCFF computed on a grid of points spaced by 5 km in latitude and longitude and the application of a smoothing algorithm. The methodology adopted in this paper assumes that earthquakes occur by rupture of rectangular faults with uniform stress drop in homogeneous elastic half-space (Console *et al.* 2008). These assumptions, which have become popular in literature, could be oversimplifying with respect to the real physical situation. For instance, the existence of competing plates with not simple geometry in the Nankai-Tokai subduction area might change the mechanical state dramatically. Moreover, the fault geometry is greatly simplified into rectangular shapes between which there may be a marked offset. For example, the boundary between Tokai and Tonankai segments could actually be more continuous than in our present calculation. Taking this circumstance into consideration, the stress concentration in the neighbouring area of the Tokai seismic source, might be supposed to be more remarkable than that shown in our results.

In our algorithm the causative sources are discretized by a dense grid of point sources uniformly distributed on the respective rectangular areas, simulating a slip variable, constant stress-drop dislocation on each source (Fig. 2). The typical spacing between the nodes of a source grid is 2 km for large magnitude events, or less for smaller magnitudes. To avoid anomalous values at points very close to a particular node of the causative faults, the points within a distance equal to the grid spacing from any of these nodes were

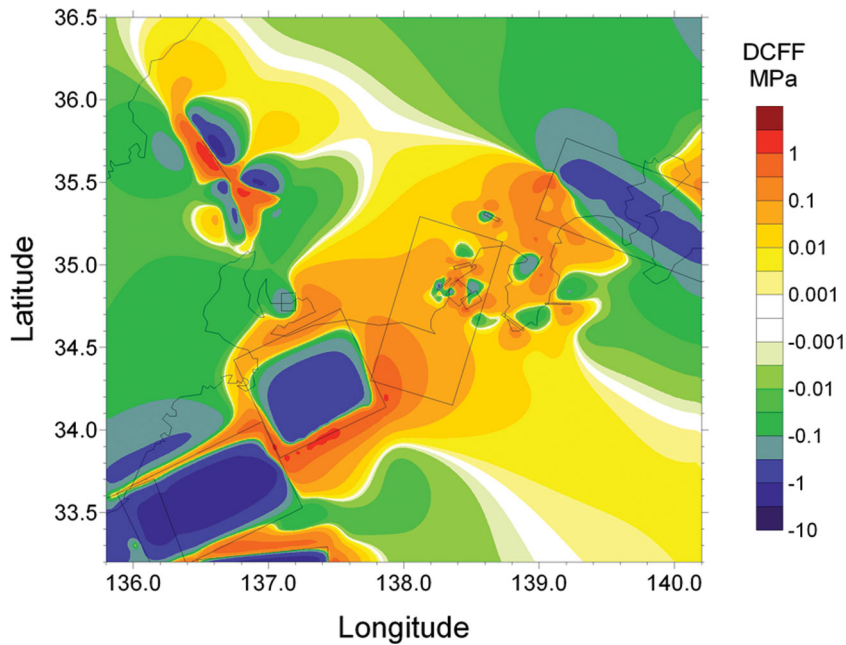


Figure 2. Coulomb stress change caused by the large earthquakes occurred on the faults surrounding the northeastern fault segment of the latest Ansei-Tokai earthquake of 1854 December 23 subsequently to this earthquake. The stress was resolved on the Tokai 1854 earthquake mechanism, at a constant depth of 20 km.

ignored, and the values were obtained by interpolation of the values on surrounding gridpoints.

The number of gridpoints falling in the rectangle of the horizontal projection of the fault rectangle was 406. Among these points, the minimum, average and maximum ΔCFF values were -0.52 MPa, 0.09 MPa and 0.66 MPa respectively. The average of the positive ΔCFF values was 0.10 MPa. Clearly, the largest positive values of ΔCFF (encouraging failure of the fault) were at parts of the segment closest to the sources of the $M7.9$ Tonankai 1944 and $M7.9$ Kanto 1923 earthquakes, located southwest and northeast of the Tokai segment, respectively. The intraplate 1891 $M = 8.0$ Nobi earthquake had only a minor negative effect (clock delay) on the stress field on the Tokai source. In fact, its minimum ΔCFF was -0.0035 MPa, with an average of -0.0013 MPa. In agreement with Mogi (1986), we found a moderate positive effect (clock advance) caused by the Nobi 1891 earthquake on the Tonankai segments. On this segment the stress interaction yielded an average positive ΔCFF (0.0013 MPa), and a maximum value of 0.0026 MPa. Clock advances and delays are calculated by dividing calculated stress changes by stressing rates inferred from stress-drop calculations.

A few negative values on the rectangular fault projection are the effect of three moderate inland and offshore earthquakes of magnitude 6.4, 6.1 and 6.4, with epicentres just inside the horizontal projection of the Tokai segment, occurred in 1935, 1965 and 2009, respectively. The effect of the latest of these earthquakes has been studied by Aoi *et al.* (2010). They concluded that the 2009 earthquake has ruptured a locked patch of the Tokai segment, increasing significantly the expected occurrence rate of the characteristic earthquake on the same segment. In agreement with these results, we note that in the map of Fig. 2 a spot of relatively large positive ΔCFF values is related to the source of the $M6.4$ 2009 earthquake in the Suruga Bay.

Adopting $\Delta CFF = 0.10$ MPa (the average of the positive values) for the computation of the equivalent clock change, we obtain a small clock advance of $\Delta t = 5.0$ yr. Applying this clock change to

modify the recurrence time T_r or the elapsed time t , as described by Console *et al.* (2008, 2010), the probability of the next characteristic earthquake for the Tokai source is estimated as 0.064 (6.4 per cent) for the period between 2010 and 2019, a marginal increase from the 6.1 per cent value calculated without interactions. The change to 30-yr probability is 19.3 per cent up from 18.7 per cent.

We cannot predict where the nucleation of the next Tokai characteristic earthquake will take place. Assuming as the most conservative solution, that the nucleation will take place on the point of the largest ΔCFF (0.66 MPa), the clock advance becomes $\Delta t = 33$ yr and the respective conditional probability for the next 10 yr equal to 7.7 per cent. The corresponding 30-yr probability value rises to 22.3 per cent.

Stress interaction does not have a strong impact on the estimate of the effect of source interaction also under the minimum rate interpretation of only three events in 1170 yr. In this case the clock advance related to the average positive ΔCFF is estimated as 11.7 yr, and the conditional probability raises to 3.1 per cent from the value of 3.0 per cent obtained without interactions. The same calculation for a 30-yr period yields 9.3 per cent. Again, we considered also the largest ΔCFF for the computation of the clock advance, obtaining $\Delta t = 77$ yr, a 10-yr probability of 3.6 per cent and a 30-yr value of 10.2 per cent.

This exercise shows that the effect of stress interactions is small in the context of the relevant differences related to the assumption of different hypotheses on the earthquake history. This is probably because of the small dip angle of the fault.

A more correct approach would require the computation of ΔCFF on the real fault surface, on the rectangle defined by the hypocenter coordinates, linear dimensions of the fault segment and its focal mechanism solution. Also in this case, we have used the same dimensions and focal mechanism as in the previous application. Fig. 3 shows the results of these computations on a map.

Among the 504 gridpoints falling in the rectangle of the fault segment, the minimum, average and maximum ΔCFF values were

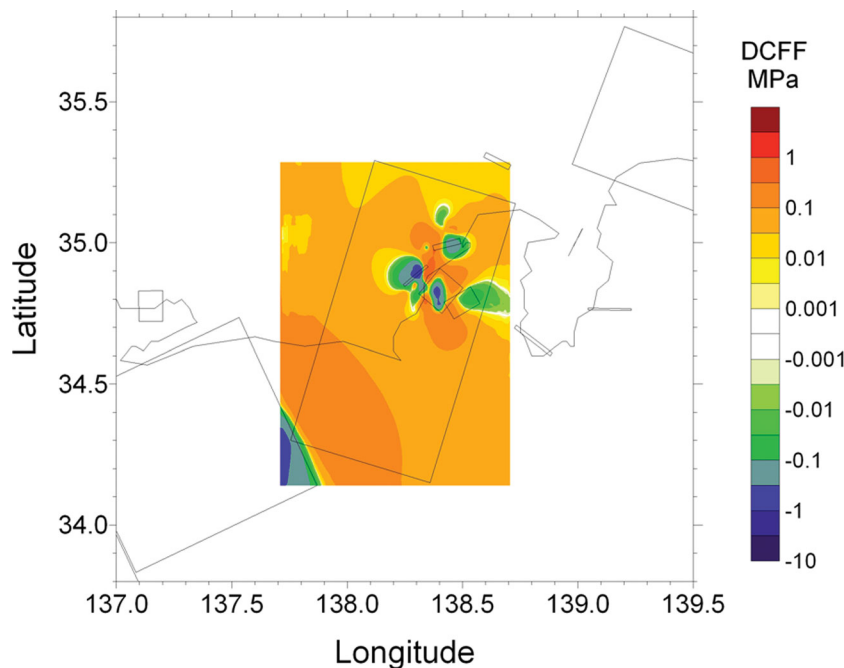


Figure 3. As in Fig. 2, with the Coulomb stress change computed directly on the rectangle of the fault segment.

−1.0, 0.076 and 0.85 MPa, respectively. The average of the positive values only was 0.095 MPa. In this case, assuming $\Delta CFF = 0.095$ MPa, the probability of the next characteristic earthquake for the Tokai source in the next 10 yr is estimated as 6.4 per cent and 3.1 per cent under the maximum and minimum rate interpretations respectively. Again, adopting $\Delta CFF = 0.85$ MPa as the most conservative solution, the same probabilities raise up to 8.0 per cent and 3.4 per cent, respectively.

While this work was nearly at its conclusion, the great $M9.0$ earthquake of 2011 March 11 took place offshore of the Tohoku coast. We included this earthquake, its $M7.3$ foreshock of March 9 and its $M7.9$ largest aftershock of March 11 in the computation of ΔCFF on the Tokai fault segment. The source parameters for these events were taken from the inversion of GPS observations as reported by Nishimura *et al.* (2011). We found that the average effect of this event was only of the order of 0.002 MPa, with a maximum value of 0.015 MPa, leading to the conclusion that it was marginal in the context of our study. This is in agreement with the results obtained by Toda *et al.* (2011). We took into consideration also the $M6.4$ aftershock occurred on 2011 March 15 near Mount Fuji, a few kilometres to the north of the northern edge of the Tokai fault considered in this study. However, also the effect of this aftershock, for which we estimated an average of the positive ΔCFF smaller than 0.001 MPa and a maximum value of 0.013 MPa, turned out as negligible.

4 METHOD OF SIMULATIONS BASED ON THE GUTENBERG–RICHTER LAW

We apply an algorithm after Parsons & Geist (2009) to simulate the spatial and temporal earthquake distribution on the Nankai, Tonankai and Tokai subduction interfaces. We calculate earthquake behaviour with a very simple model that uses the fewest and most robust observational parameters as possible. The simulation is based on two data classes (slip rates, magnitude–frequency distribution)

and is described by five parameters/assumptions: (1) we match long-term geological slip, or geodetic rate to at least within 10 per cent of quoted values (assuming that ± 10 per cent is about the precision on rate measurements), (2) we hold the magnitude–frequency distribution to be as close as possible to a linear Gutenberg–Richter relation (Ishimoto & Iida 1939; Gutenberg & Richter 1954) with b -value (slope) of 1.0 over a magnitude range $M \sim 5.8$ – 8.8 , (3) we use an empirical magnitude–area relation (Wells & Coppersmith 1994) to describe the spatial extent of ruptures, (4) we calculate mean event slip from the moment–magnitude relation (Hanks & Kanamori 1979) assuming a shear modulus of $\mu = 30$ GPa and (5) we allow ruptures to jump over an adjustable distance (5 km; Barka & Kandinsky-Cade 1988; Harris 1992; Harris & Day 1993, 1999; Lettis *et al.* 2002).

The simulator can be thought of as a spatial seismic gap model. We select a model duration, and then calculate the cumulative slip budget available at each point in the model. We then populate the model faults with earthquake ruptures until the slip budget is used up. If a lot of slip has already occurred in one part of the model fault(s), then the routine seeks to put the slip elsewhere (into a gap). Because we assign initial rupture locations with a degree of randomness, we must make multiple simulations to reduce the influence of the starting rupture locations. We include ruptures from a lower threshold of $M = 5.79$, which is governed by the model discretization, up to $M = 8.74$, which represents the entire area of the subduction zone.

We divide the 650-km-long Nankai-Tonankai-Tokai subduction front (Fig. 1) into $5 \text{ km} \times 5 \text{ km}$ patches, which are slightly smaller ($M = 5.49$) than the smallest earthquake rupture areas that we include, which are made up of two patches ($M = 5.79$). All larger ruptures consist of combinations of contiguous patches, where contiguous means adjoining patches, or patches within the allowable jump distance (5 km in this instance; Barka & Kandinsky-Cade 1988; Harris 1992; Harris & Day 1993, 1999; Lettis *et al.* 2002). We treat the locked seismogenic zone as 60-km wide on average (e.g. Sagiya & Thatcher 1999; Mazzotti *et al.* 2000; Hori *et al.*

2004; Ito & Hashimoto 2004; Wang *et al.* 2004). Although the Nankai-Tokai zone has defined segments (Ando 1975b; Ishibashi & Satake 1998), no fault interruptions or slip barriers are imposed in the model. The only difference along strike is the slip rate, which we apply according to Ishibashi & Satake (1998) as modified by Mitsui & Hirahara (2004) (Fig. 1); there is a significant gradient in slip rate that ranges from 60 mm yr⁻¹ at the west end of the zone to 20 mm yr⁻¹ in the east, which is defined over 150–200 km segments (labelled A, B, C, D and E in Fig. 1). For the model, we use constant slip rate in each segment. The actual Nankai-Tokai trough and subduction zone changes orientation along strike; however, we assume that the given slip-rate vectors are parallel to earthquake rake directions. We thus display the subduction zone as a simple linear feature (Fig. 1). Our model does not extend southwest into the Kyushu subduction zone.

We begin to populate the simulation with earthquake ruptures by assigning earthquake nucleation sites distributed in proportion to slip rates, such that the highest slip rate parts of the fault are likely to nucleate the most events. Hypocenter locations are drawn at random from the spatial distribution, and their magnitudes are randomly sampled from a Gutenberg–Richter distribution. Hypocenter assignment is only governed by the overall slip rate and not by previous earthquake slip, except in the case where the whole slip budget is already used up. As will be described, rupture growth is affected by past earthquake slip.

Rupture areas are determined from an empirical magnitude–area relation (Wells & Coppersmith 1994). Mean event slip (\bar{S}) is calculated through the moment–magnitude relation of Hanks & Kanamori (1979) assuming a shear rigidity of $\mu = 30$ GPa as

$$\bar{S} = \frac{10^{(1.5M+9.05)}}{\mu A},$$

where A is rupture area. Contiguous, uniform-slip ruptures are initially allowed to grow at random into adjoining patches until they cover their magnitude-appropriate areas. Each patch of an individual rupture has the same amount of slip. As more ruptures are added, they continue to grow at random, but if a patch with pre-existing slip accumulation is encountered, then rupture growth is sent to a

different patch. If all patches have pre-existing slip, then growth occurs into the patch with the least accumulated slip. If more than one equal least-slip patch choice is possible, then the decision is made at random.

We allow ruptures to grow into patches with the least accumulated slip under the assumption that lowest prior slip implies highest failure stress. Should this occur at a boundary where slip rates change significantly, slip can end up preferentially assigned to the lower slip rate fault early in the simulation. As the model is updated, if a hypocenter is assigned at a site that produces cumulative slip anywhere within its rupture that exceeds the cumulative long-term slip constraint (plus 10 per cent uncertainty), that event is repeatedly moved to new locations until all of its slip can be accommodated. No step-overs or junctions occur in our Nankai-Tokai trough model; however, the method does allow ruptures to jump between fault branches or over fault patches with large accumulated slip within a given distance. The decision whether a rupture jumps over a patch is governed by the same concept of rupture growth, using the pre-existing slip distribution under the assumption that high slip implies low failure stress; modelled dynamic rupture jumps are shown to be most encouraged by a high stress state (e.g. Harris & Day 1993, 1999).

Ruptures continue to occur in the simulation until the accumulated slip rate constraints are met (Fig. 4). For the Nankai-Tokai trough we simulate 5000-yr periods, which means the westernmost part of the zone acquires 300 m of total slip (± 10 per cent), whereas the easternmost (Tokai) zone acquires 100 m (± 10 per cent). Some changes to the input magnitudes are required because, towards the end of a 5000-yr simulation, a randomly drawn rupture may not be able to be fit within the already accumulated slip. If a rupture magnitude is drawn from the Gutenberg–Richter distribution that exceeds the available area, then its magnitude is reduced. If a reduced event still cannot be fit after 1000 attempts at different sites, this means that the entire slip budget is used up and the simulation ends. Some magnitudes are missing from the magnitude–frequency distribution on the lowest end because of the 5 km \times 5 km fault discretization, which forces the minimum magnitude (two patches) to be $M = 5.79$ and then the next size up to be $M = 5.97$.

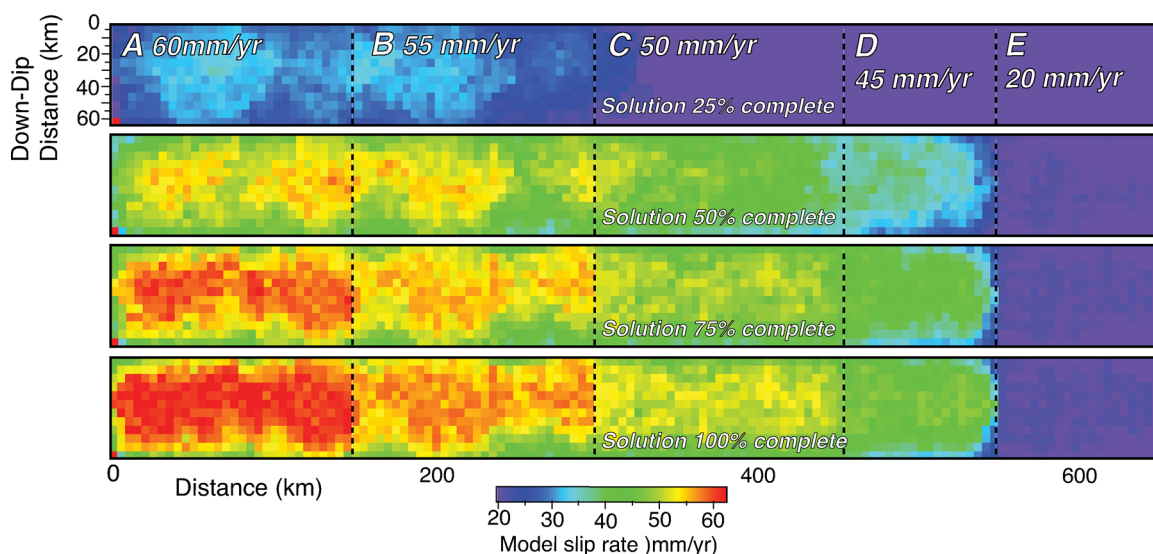


Figure 4. Accumulated slip during one model run showing slip status at 25 per cent, 50 per cent, 75 per cent and 100 per cent completion. Hypocenter initiation is preferentially distributed into segments with highest observed slip rates. Ruptures grow into regions with least accumulated slip, which is a proxy for greatest failure stress.

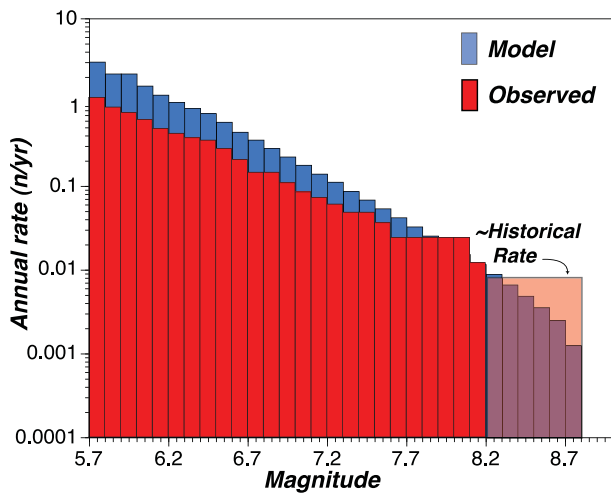


Figure 5. Blue columns show cumulative average magnitude–frequency distribution output from 100 simulations covering the range from $M > 5.7$ to 8.7. Model fault discretization causes the lowest magnitudes to be fixed at $M = 5.79$ and $M = 5.97$ leaving no contribution from the $M = 5.8$ to 5.9 bin. Red columns show the observed annual rate based on 83 yr of instrumental seismicity in the boxed area shown in Fig. 1, and the shaded area gives the approximate historical rate assuming a 150 yr open interval before AD684, and a magnitude range from $M \geq 8.2$ to $M \leq 8.8$. The Gutenberg–Richter model produces about 2.5 times the rate of observed mid-magnitude events, including 3.04 $M = 5.79$ per yr. Applying the same open interval used to define the observed catalogue period, then the simulation produces 28 $M \geq 7.9$, 18 $M \geq 8.1$, 10 $M \geq 8.3$ and 5 $M \geq 8.5$ quakes as compared with the observed 12 (Table 1). Thus the rates are comparable if the historical completeness threshold is between $M = 8.1$ and 8.3.

We emphasize a Gutenberg–Richter constraint because in information-poor settings, for which the technique is intended, it provides a simple governing relation for magnitude distribution. For smaller magnitudes, individual fault zones display such behaviour in their magnitude distributions (e.g. Abercrombie & Brune 1994; Westerhaus *et al.* 2002; Schorlemmer *et al.* 2003; Wyss *et al.* 2004; Schorlemmer *et al.* 2004). Less well understood is whether there is departure from the linear magnitude–frequency trend at larger magnitudes into characteristic earthquakes (Schwartz & Coppersmith 1984; Wesnousky 1994), or whether the linear trend is maintained across the entire magnitude range (Stein & Newman 2004; Stein *et al.* 2005). Indeed this issue prompted a formal debate at the 2010 Seismological Society of America Annual Meeting (Schwartz 2010; Page 2010), and will require additional research to settle. The Nankai region as a whole demonstrates Gutenberg–Richter behaviour up to at least $M = 7.5$ —the magnitude distribution of the earthquakes mapped in Fig. 1 is shown in Fig. 5—however, not all of these events occurred on the interplate contact.

We reencounter a persistent and difficult issue in seismology with regard to matching the long-term rate of the largest earthquakes with instrumental recordings of smaller events regardless of whether we assume a Gutenberg–Richter or characteristic magnitude–frequency distribution in that there are more large palaeoevents than instrumental seismicity would imply. One explanation might be that the maximum magnitude is much higher than has been observed since AD684, which would mean more seismic moment is absorbed by infrequent larger earthquakes than our model produces. However, the instrumental and model rates do match in the interval between $M \sim 7.8$ –8.2 (Fig. 5). This raises the question whether the instrumental catalogues are really complete; for example, examination of

Fig. 1 shows that, other than the 1946 $M = 8.1$ Nankaidō earthquake, segment A has experienced zero $M \geq 5.6$ earthquakes since 1926. This seems an unlikely long-term behaviour, but we cannot know for certain. In addition, earthquake rates might branch into long-term cycles of increased or diminished activity owing to fault interactions (e.g. Marzocchi & Lombardi 2008). We therefore take the long-term plate motion rates to be a better estimate of expected earthquake rates than present-day seismicity.

The debate whether individual faults exhibit Gutenberg–Richter magnitude–frequency behaviour may not be important with regard to our simulations. We assume for the calculations that all earthquakes occur on a single plane that perfectly accounts for observed convergence rates. However, in reality, a broader network of faults that extends into the crust accommodates this strain. Therefore, it is possible that a mixture of characteristic faults (e.g. Wesnousky 1994; López-Ruiz *et al.* 2004) or Gutenberg–Richter distributed faults with different maximum magnitude cut-offs (e.g. Kagan 2002a,b) can satisfy the linear power-law trend. Our solution for regional earthquake rates can be considered one for the volume that contains the interplate contact, that accommodates the full plate convergence, and that is observed to have Gutenberg–Richter behaviour (Fig. 5). That is, we can think of our simple planar-fault model as simulating crustal, upper mantle and interplate-contact earthquakes that accomplish convergence on different planes.

5 SIMULATOR RESULTS

Our simulations yield spatial distributions and rates of earthquake ruptures from $M \geq 5.79$ to $M \leq 8.74$. We emphasize the largest ($M \geq 7.9$) ruptures here, which we can compare with the historical and palaeoseismic record (Ishibashi & Satake 1998). Magnitude 7.9 has the potential to cause considerable shaking and tsunami damage in the adjacent areas, as well as in Tokyo (e.g. Furumura & Saito 2009). We show example fits to the observed slip rate constraints (Fig. 4), and an example participation distribution of $M \geq 7.9$ ruptures (Fig. 6). The purpose of our simulations of Nankai–Tokai subduction zone earthquakes is to produce an estimate of the possible ruptures and their spatial rate variability. Unlike many of the world’s plate boundaries, a comparably lengthy palaeorecord (Ishibashi & Satake 1998) of past earthquakes exists for comparison with the simulation results.

From hundred 5000-yr simulations, we develop a catalogue of 9447 $M \geq 7.9$ earthquakes along the Nankai, Tonankai and Tokai zones. As would be expected, the highest number of simulated ruptures involves the western Nankai (segments AB) zone (Figs 4 and 6), which has the highest slip rates (60–55 mm yr^{-1} ; Fig. 1). The simulator model is unsegmented in that no structural barriers to slip are imposed other than the slip rate boundaries. By contrast, the Nankai–Tonankai historical catalogue is interpreted as an example of characteristic earthquakes from a highly segmented fault (Fig. 1). In a past study, a theoretical Gutenberg–Richter magnitude–frequency distribution was able to reproduce characteristic slip-per-event observations (Parsons & Geist 2009); one of our key goals in this study is to compare spatial rupture distributions between simulated and observed to determine the extent to which a Gutenberg–Richter distribution might explain the historical catalogue.

We examine the slip distribution of each earthquake to compare the simulated catalogue of segment ruptures with observed. If a simulated $M \geq 7.9$ event has accumulated a rupture area covering at least 50 per cent of one of the identified segments (A–E) we consider that segment involved in the simulated earthquake. This criterion

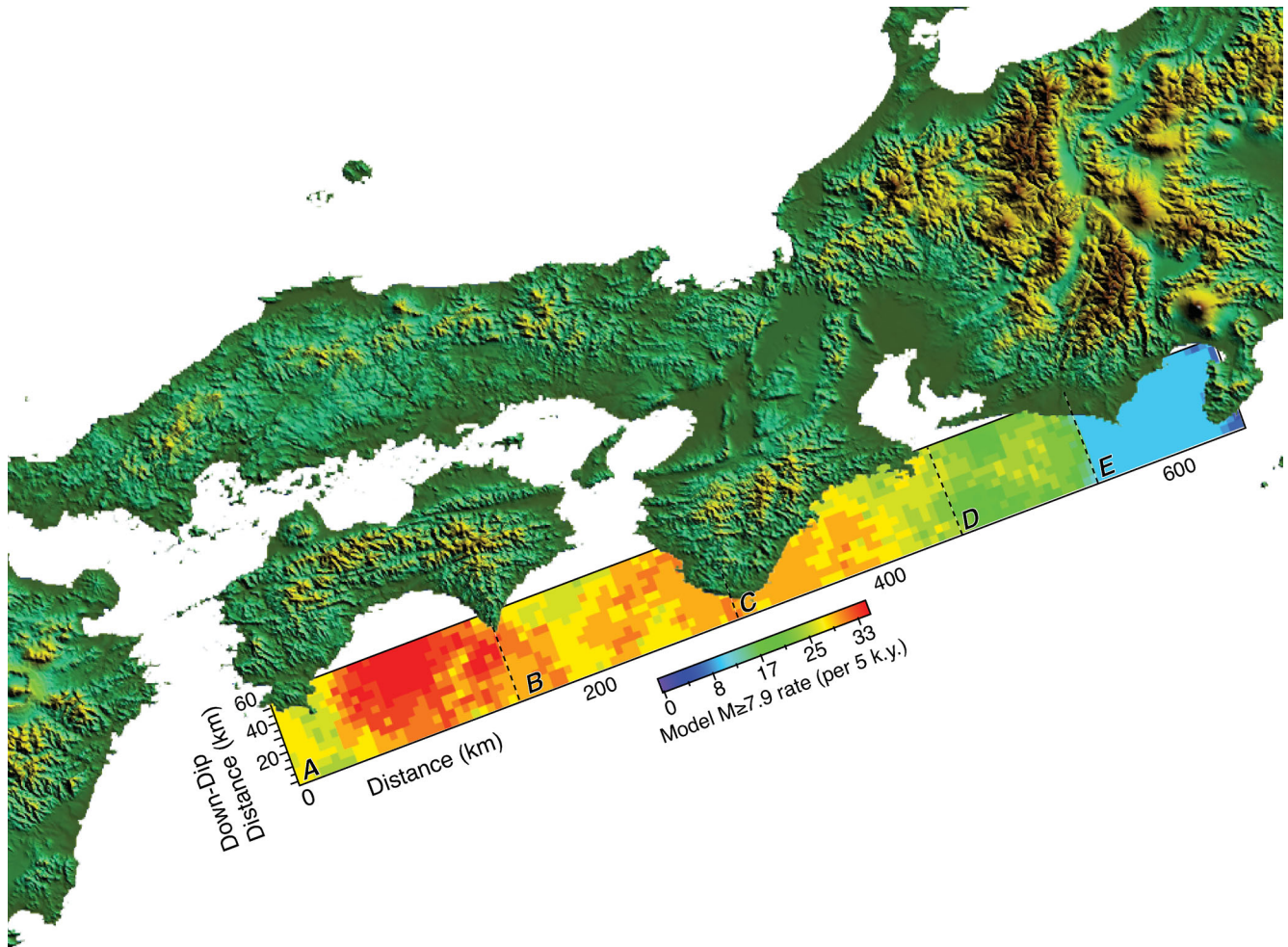


Figure 6. Example plots of participation rates of $M \geq 7.9$ earthquake ruptures in $5 \text{ km} \times 5 \text{ km}$ cells over a 5000-yr period. Participation rates in this example range from 7 to 36 in 5000 yr, depending on location and slip rate.

is based on the minimum thresholds of identification from macroseismic intensity and tsunami wave height (e.g. Ishibashi & Satake 1998) for comparison with the historic catalogue. The relative concentration of simulated ruptures on identified segments can be assessed in Fig. 7; from hundred 5000-yr simulations, the percentages of involved segments are plotted for different lower magnitude cut-offs. As would be expected, smaller magnitude ($M \geq 7.9$) events are more uniformly distributed over all segments (roughly in proportion to slip rate; Fig. 7). Higher magnitude events require larger rupture areas, and thus must occur on multisegment combinations.

The most characteristic interpretation of the historical earthquake segment distribution (blue columns on Fig. 7) shows far fewer segment combinations than the Gutenberg–Richter simulation results. However, for valid comparison, two factors must be accounted for: (1) there is uncertainty about which segments were involved, particularly for the oldest events in the record, and (2) the combined simulator results cover a longer time (100 times 5000 yr), than the 1326-yr (AD684–2010) Nankai catalogue and thus might be expected to have more variability. We therefore establish confidence bounds on segment assignments both from the historical catalogue, and the simulations.

We infer 12 individual large earthquakes since AD684 from the summary by Ishibashi & Satake (1998), and their possible segment rupture extents are given in Fig. 1. From the location and

segment-assignment uncertainties we find that there can be at least 72 different segment rupture combinations. In Fig. 8, we show the mean number of observed segment ruptures along with 95 per cent confidence bounds calculated from the 72 possible combinations. The most commonly observed historical ruptures are those across the western Nankai-Tokai zone (segments AB), and the second most commonly observed historical events are complete ruptures across all zones (segments ABCDE); no single-segment ruptures are interpreted to have ever happened in the historical catalogue. For comparison, we generated 100 sets of 12 ruptures drawn from the 9447 $M \geq 7.9$ simulated events, as well as for higher magnitude cut-offs (Fig. 8). We find that the simulator results fit observed rates within 95 per cent confidence bounds for $M \geq 8.1$ and $M \geq 8.3$ events, and for all except segment CDE earthquakes at $M \geq 7.9$.

We note some similarity in the overall shape of the segment rupture rates between observed and those calculated from simulations, particularly for larger magnitudes (Fig. 8); $M \geq 8.2$ ruptures fit the observed segment distribution within the narrower 67 per cent confidence bounds except for CDE ruptures (Fig. 9); the historical catalogue allows for many scenarios that include segment E involvement, which is hard to match at 67 per cent confidence with the simulator constrained at the slow (20 mm yr^{-1}) convergence rate on that segment.

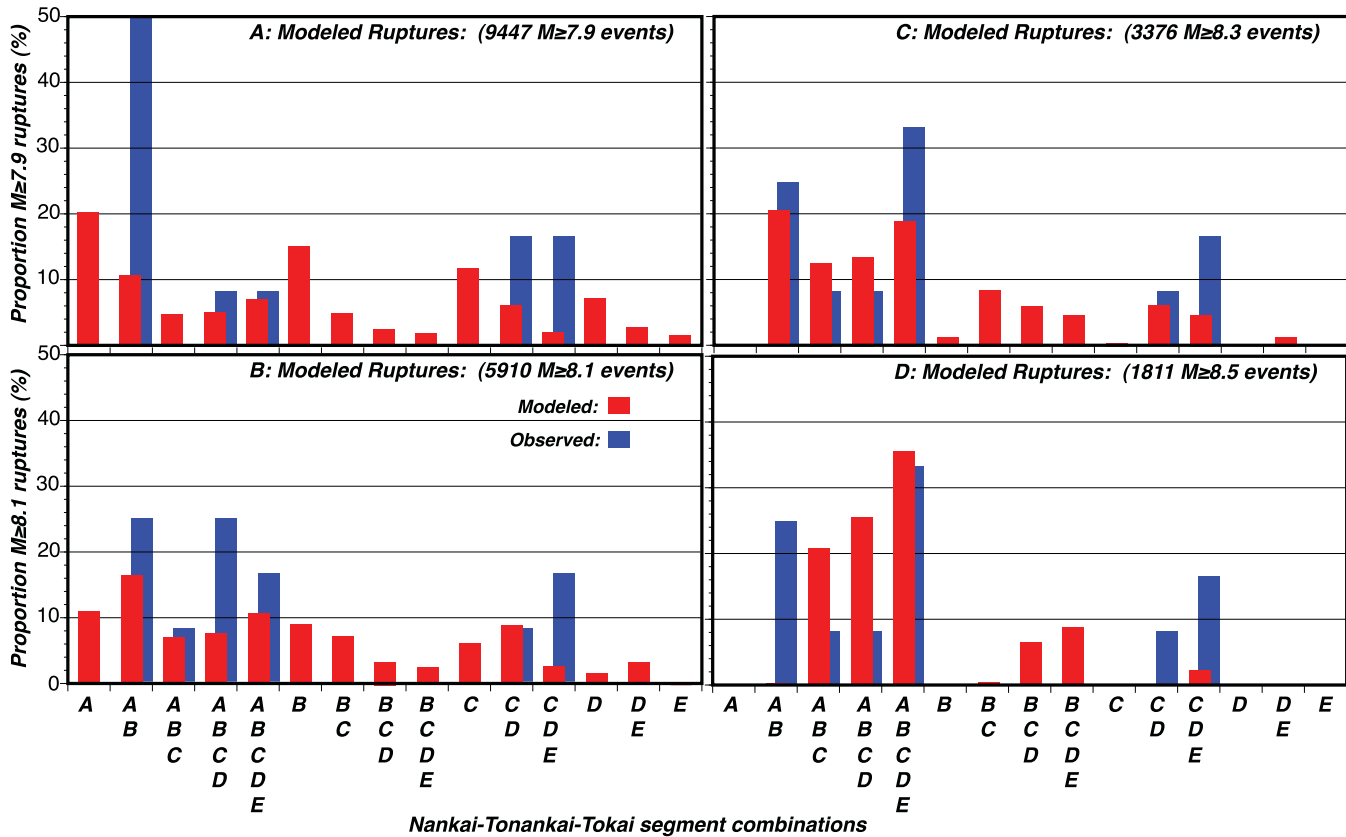


Figure 7. Red columns show distributions of simulated $M \geq 7.9$, $M \geq 8.1$, $M \geq 8.3$ and $M \geq 8.5$ earthquakes on Nankai (segments AB), Tonankai (segments CD) and Tokai (segment E) zones. We assign ruptures to a defined segment if its spatial extent occupies at least half of the segment area. Rupture proportion by zone is calculated from percentage of the total number of ruptures. Blue columns show three different characteristic interpretations of the historic catalogue from the three columns given in Fig. 1 by assigning the smallest potential ruptures in (a), moderate in (b), and the largest interpretations in (c) and (d). Simulations most closely match an interpretation of the historic catalogue with a lower threshold of $M \geq 8.3$.

Twelve events is a small sampling with which to characterize long-term earthquake behaviour, and the ability of a Gutenberg–Richter distribution to reproduce the segment distribution of earthquake ruptures at 95 per cent confidence raises a question. Does the necessary bias of historical and palaeoseismology towards the largest magnitude events combined with a strong slip-rate gradient along the Nankai zone create the appearance of characteristic earthquakes? We have no comparably long record of smaller events and their magnitude distribution. The largest earthquakes require multiple segment areas to rupture, and because there is a much faster slip rate to the southwest, there can only be a limited number of observable combinations.

We show that a simple, slip-rate-based earthquake simulator can produce a segment distribution of high-magnitude ruptures that is consistent with the parent distribution from which the historic and palaeoearthquake record could have emerged. We thus use the simulator results to explore large earthquake rate calculations for the Nankai, Tonankai and Tokai subduction zones.

6 SIMULATOR-BASED EARTHQUAKE RATE CHARACTERISTICS

We use the results of hundred 5000-yr simulated earthquake catalogue to calculate mean rates of large ($M \geq 7.9$) earthquakes. Taking the inverse of the simulator rates yields mean recurrence intervals (Table 2), this can be used to calculate earthquake proba-

bility. Use of 100 simulations gives an estimate of the rate variability that can satisfy the long-term slip-rate data; the intervals bounding 95 per cent and 67 per cent of the calculated values are also given in Table 2.

Not surprisingly, we calculate the shortest intervals on the highest slip-rate segment (segment A), with proportional increase corresponding to the decreased slip rates to the northeast (segment E). This is especially evident when smaller magnitude events (threshold $M \geq 7.9$) are included (Table 2). Our calculations show segment B to have the shortest intervals for larger, multisegment earthquakes even though it has a slightly slower slip rate than segment A (55 mm yr^{-1} compared with 60 mm yr^{-1}). This result is an artefact of the simulation model having no extension southwestwards into the Kyushu subduction zone, making very large earthquake growth asymmetric and thus slightly more difficult.

Here we compare segment event intervals (inverse of rate) between the mean calculated from the Gutenberg–Richter simulation and the range calculated with the historical catalogue using the time-predictable model. As discussed previously, there is more than one interpretation of the segment assignments in the historical catalogue, so we calculate minimum and maximum rates for involvement of each segment (Table 2).

We find agreement between the Gutenberg–Richter segment intervals and the historical catalogue. All modelled segment intervals overlap with the maximum rate historical interpretation across their 67 per cent ranges (Table 2; Fig. 10). The maximum rate historical interpretation overlaps the Gutenberg–Richter simulated intervals

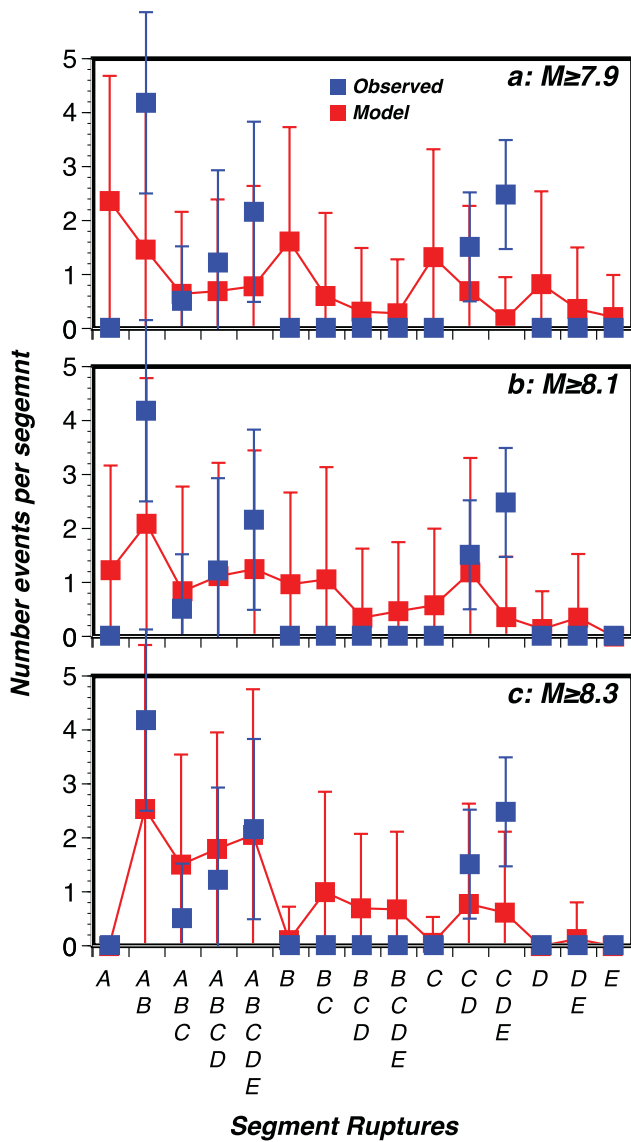


Figure 8. Observed mean rupture distribution by segment (Ishibashi & Satake 1998; blue squares) and 95 per cent confidence bounds based on location uncertainties. Actual magnitudes of historic events are not known, but likely fall within the range of model results shown. Also shown are mean numbers of segment ruptures from 100 random draws of 12 events from (a) $M \geq 7.9$ ruptures developed from simulator calculations (red squares). In (b) the same results are shown except with calculated numbers of $M \geq 8.1$ events. In (c) the distribution of $M \geq 8.3$ events is shown. The simulator results show that Gutenberg–Richter magnitude–frequency cannot be ruled out as a parent distribution of the observed catalogue at 95 per cent confidence for $M \geq 8.1$.

if the broader 95 per cent ranges are considered for all segments except segment E, which cannot be matched to the maximum rate interpretation for that segment. We encounter this difficulty because our calculations are fit to the significantly slower slip rates on segment E (20 mm yr^{-1} compared with 60 mm yr^{-1} on segment A). This threefold slip-rate difference is not manifested in the historical catalogue, which under the maximum rate interpretation has mean intervals only 1.5 times longer than segment A. The minimum rate interpretation shows segment E intervals 2.2 times longer than segment A (Table 2) instead of the three times longer interval expected from slip-rate variation.

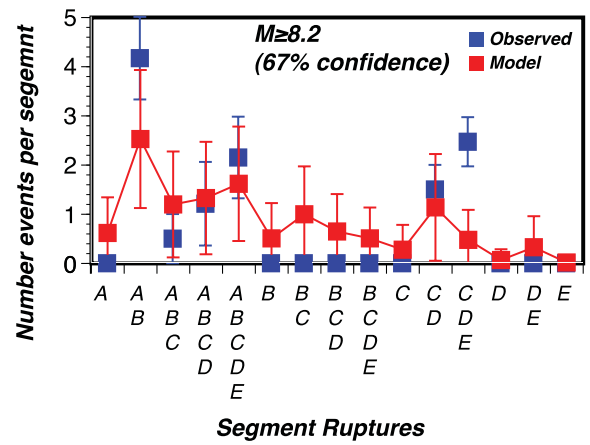


Figure 9. Observed mean rupture distribution by segment (Ishibashi & Satake 1998; blue squares) and 67 per cent confidence bounds based on location uncertainties. Also shown are mean numbers of segment ruptures from 100 random draws of 12 $M \geq 8.2$ events. All segments are fit except for CDE ruptures.

Table 2. Calculated mean recurrence intervals for simulated earthquakes of varying magnitude thresholds involving the five segments along the Nankai–Tonankai subduction zone. Segment rates depend on how involvement is defined. We take this to be 50 per cent of the segment rupture area.

Segment	Simulation Intervals (yr)				
	A	B	C	D	E
$M \geq 7.9$					
Mean	123	112	129	178	460
95 per cent	94–161	94–131	104–166	147–226	309–600
67 per cent	104–139	102–122	119–139	151–191	378–537
$M \geq 8.1$					
Mean	175	140	160	232	671
95 per cent	128–248	111–178	128–216	161–329	378–781
67 per cent	142–207	125–151	142–172	184–275	444–698
$M \geq 8.3$					
Mean	266	192	221	461	789
95 per cent	178–378	142–261	166–309	207–486	444–918
67 per cent	207–309	161–216	184–248	241–379	537–821
Calculated intervals from max. rate historical catalogue (yr)					
Segment	A	B	C	D	E
Mean	158	158	180	180	234
95 per cent	43–273	43–273	~0–398	~0–398	34–434
67 per cent	100–215	100–215	71–289	71–289	134–334
Calculated intervals from min. rate historical catalogue (yr)					
Mean	180	180	235	235	390
95 per cent	55–305	55–305	~0–505	~0–505	~0–991
67 per cent	118–242	118–242	100–370	100–370	90–690

The effect of longer intervals between large earthquakes involving the Tokai segment (E) in the Gutenberg–Richter simulation model is a lower implied earthquake hazard. In the following section, we compare probability calculations made using the time-predictable model with those taken from calculated large earthquake rates derived from the simulations.

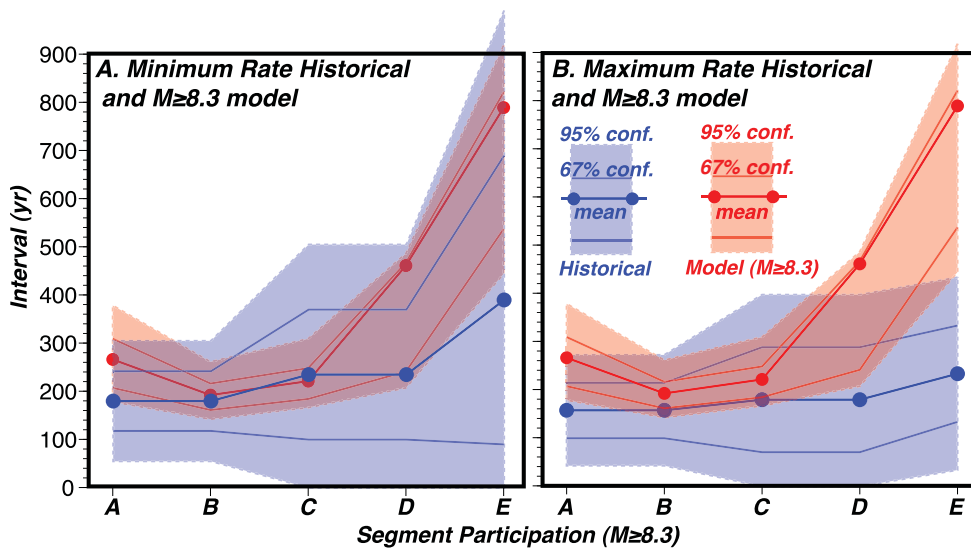


Figure 10. Graphical view of calculated mean recurrence intervals for simulated $M \geq 8.3$ earthquakes involving the five segments along the Nankai-Tonankai subduction zone. Modelled segment participation intervals are compared with (a) the minimum rate interpretation of the historical catalogue (Fig. 1), and (b) the maximum rate interpretation. The intervals overlap at 95 per cent confidence except for the maximum rate interpretation for segment E intervals.

7 COMPARISON OF TIME-PREDICTABLE AND SIMULATOR-MODEL DERIVED EARTHQUAKE PROBABILITY FOR THE TOKAI SEGMENT

$M \geq 7.9$ involvement intervals for segments A–D from the simulations match minimum and maximum rate interpretations from the historical catalogue (Table 2; Fig. 10), as well as the spatial distribution of segment ruptures (Fig. 8) and thus produce the same time-dependent and time-independent probability values. As this paper is, in part, an evaluation of the applicability of simple rupture simulations for forecasting, we focus on the differences between the renewal-characteristic approach and the Gutenberg–Richer distributions, which are primarily identified on the Tokai segment (segment E; Fig. 1).

The probability of an earthquake in which the Tokai segment participates was calculated using a time-predictable interaction method after Console *et al.* (2008, 2010). We obtained two different results with: (1) a maximum rate interpretation involving the Tokai segment (E) rupturing entirely six times after 786 A.D., and (2) in a minimum rate interpretation, only three Tokai times in the same period. The probability of the next event in 30 yr based on a maximum rate (recurrence parameters of $T_r = 234$ yr, $\alpha = 0.428$) is 18.7 per cent. This probability rises up to 19.3 per cent under the assumption of a clock change based on the largest value of ΔCFF on the fault. The 30-yr probability from the minimum rate interpretation (recurrence parameters of $T_r = 390$ yr, $\alpha = 0.77$) is 9.3 per cent or 10.2 per cent with earthquake interactions.

The 30-yr probability values ($M \geq 7.9$) calculated from simulator-based recurrence are much lower than those calculated from the maximum rate time-predictable model (5–13 per cent versus 18–19 per cent in 30 yr), and do not overlap at 95 per cent confidence. The reason for this is that the recurrence intervals are shorter from the time-predictable analysis (234–390 yr versus 307–600 yr), which leads to higher time-dependent probability values. The lower preferred probability of 9–10 per cent in 30 yr from the minimum rate interpretation is essentially the same as the simulator-based

mean of 9 per cent in 30 yr for $M \geq 7.9$ (95 per cent confidence range is 5–13 per cent) if the coefficient of variation is high ($\alpha = 0.9$; Table 3), though the historical catalogue is likely incomplete at $M \geq 7.9$. The two methods have comparable probabilities at 95 per cent confidence for simulator results for $M \geq 8.1$ (9–10 per cent compared with 4–10 per cent) if $\alpha = 0.9$.

A key reason for the different probability results between the two models lies in the interpretation of moment balancing. As described in the preceding section, the maximum rate historical catalogue interpretation has segment E involved interevent times that are only 1.5 times longer than segment A-involved recurrence times, whereas segment E slip rates are three times slower. One would expect interevent times of same-magnitude events to vary linearly with slip rate, whereas the historical interpretation has similar earthquake rates along the Nankai zone despite significant slip-rate variation. This interevent time discrepancy cannot be explained by smaller magnitude earthquakes on segment E because it is only involved in very large CDE and ABCDE earthquakes in the historical catalogue (Fig. 1). Given the historical nature of the events in question and the indirect observation of event slip, this source of uncertainty remains difficult to resolve.

8 DISCUSSION AND CONCLUSIONS

The controversy whether characteristic or Gutenberg–Richter magnitude distributions apply to individual faults has been going on many years, and the choice affects not only earthquake probabilities and seismic hazard calculations, but also our understanding of the physics of earthquakes and their upper magnitude limits. According to the characteristic earthquake hypothesis, the earthquake hazard is small immediately following the previous large earthquake and increases with time since the latest event on a certain fault or plate boundary. Hence, earthquake occurrence can be regarded as a quasi-periodic process (McCann *et al.* 1979; Shimazaki & Nakata 1980; Nishenko & Buland 1987; Nishenko 1991). Kagan & Jackson (1991) tested this hypothesis for earthquakes on the circum-Pacific belt using an ensemble of seismic zones because of the shortness

Table 3. Calculated 30-yr probability of involvement of segments A–E in earthquakes with minimum magnitude thresholds ranging from $M \geq 7.9$ to $M \geq 8.3$. The calculations are made with a Brownian Passage Time distribution using mean rates given in Table 2, and aperiodicity (α) values of 0.2, 0.5 and 0.9. Confidence bounds are approximated by giving the ranges within which 95 per cent and 67 per cent of calculations fall.

30-yr probability of segment involvement (per cent)					
	Segment: A	B	C	D	E
$M \geq 7.9$					
Mean $\alpha = 0.9$	28.3 per cent	30.4 per cent	27.2 per cent	20.3 per cent	8.0 per cent
95 per cent	22.4–34.4	26.9–34.4	21.8–32.0	15.3–24.4	5.3–12.5
67 per cent	25.6–32.1	28.5–32.6	25.6–29.0	18.8–23.8	6.4–10.1
Mean $\alpha = 0.5$	29.1 per cent	34.1 per cent	27.3 per cent	12.7 per cent	2.9 per cent
95 per cent	16.0–43.6	25.8–43.6	15.4–38.7	5.5–20.8	0.8–10.5
67 per cent	22.8–38.1	29.5–39.2	23.6–31.5	10.2–19.6	1.4–6.0
Mean $\alpha = 0.2$	12.5 per cent	24.7 per cent	9.9 per cent	0.2 per cent	~0
95 per cent	0.6–56.2	7.1–56.2	0.5–41.0	~0–2.6	~0–0.7
67 per cent	3.8–37.3	13.3–40.9	4.8–18.8	~0–1.8	~0
$M \geq 8.1$					
Mean $\alpha = 0.9$	20.5 per cent	25.4 per cent	14.8 per cent	14.8 per cent	4.3 per cent
95 per cent	13.3–27.4	20.2–30.6	8.4–22.4	8.4–22.4	3.1–10.1
67 per cent	17.0–25.1	23.8–28.0	11.5–19.6	11.5–19.6	4.0–8.3
Mean $\alpha = 0.5$	12.7 per cent	22.5 per cent	17.0 per cent	4.9 per cent	0.4 per cent
95 per cent	3.3–27.0	12.0–34.6	6.5–27.7	0.8–16.7	0.1–6.0
67 per cent	7.2–21.8	18.9–28.2	6.0–14.0	2.2–11.4	0.3–3.4
Mean $\alpha = 0.2$	0.2 per cent	3.5 per cent	0.8 per cent	~0 per cent	~0 per cent
95 per cent	~–8.8	0.1–26.1	~0–10.6	~0–0.8	~0
67 per cent	~0–3.0	1.4–10.9	0.3–3.8	~0–0.1	~0
$M \geq 8.3$					
Mean $\alpha = 0.9$	11.9 per cent	18.6 per cent	15.8 per cent	3.8 per cent	3.1 per cent
95 per cent	6.1–20.2	12.3–25.1	9.4–21.8	3.2–17.1	2.1–8.3
67 per cent	9.2–17.0	16.1–22.4	13.5–19.6	3.6–14.0	2.8–6.4
Mean $\alpha = 0.5$	2.3 per cent	9.4 per cent	6.0 per cent	0.1 per cent	0.1 per cent
95 per cent	0.2–12.0	2.6–21.8	1.1–15.4	~0–7.7	~0–3.4
67 per cent	1.0–7.2	6.1–16.0	3.6–11.4	~0–4.1	0.1–1.4
Mean $\alpha = 0.2$	~0 per cent	~0 per cent	~0 per cent	~0 per cent	~0 per cent
95 per cent	~0–0.1	~0–3.0	~0–0.5	~0	~0
67 per cent	~0	~0–0.6	~0–0.1	~0	~0

of the seismic record within a single zone. Their result did not support the seismic gap hypothesis, as the fault segments that had experienced higher activity in the prior period were also the most active during the test period.

The controversy between the characteristic and Gutenberg–Richter models was partly developed through discussions by Nishenko & Sykes (1993), Jackson & Kagan (1993), Kagan & Jackson (1995) and Rong *et al.* (2003). This debate did not have a clear conclusion and is ongoing. However, the recent great $M = 9.1$, 2004 Sumatra and $M = 9.0$, 2011 Tohoku earthquakes do not seem to fit the definitions of characteristic earthquakes that were expected in their respective regions. The approximate interval between great earthquakes in the Nankai zone is about 150–600 yr, meaning that empirical resolution of this issue could require many hundreds of years.

This paper is aimed at comparing forecast tools and at contributing to the magnitude–frequency debate by contrasting results obtained from two different methods in a region where reliable in-

formation on a sequence of large magnitude historical earthquakes is available.

We have first applied an already consolidated methodology for the computation of the occurrence probability of the future characteristic earthquake on the Tokai segment of Nankai–Tokai subduction fault zone (Working Group on California Earthquake Probabilities (WGCEP) 1995, 2003; Stein *et al.* 1997; Matthews *et al.* 2002). This computation assumes the validity of the characteristic earthquake model for which the earthquake may occur only on predetermined sources and its probability is conditional to the time elapsed since the last characteristic earthquake on the fault, taking also into account the history of the following events on the neighbouring active sources.

Our calculations show that earthquake interaction effects in this region are small when compared with the uncertainties affecting the statistical model used for the basic time-dependent hazard assessment. With these methods we calculate that the Tokai segment (segment E) has a 10–19 per cent rupture probability during the

next 30 yr, depending on how the historical catalogue is interpreted; we find the range of recurrence intervals to be 234–390 yr.

It should be noted that, as reported in Section 3, the probabilities obtained in this study are significantly larger than those appearing in the forecasts released by the Headquarters for Earthquake Research Promotion. The larger values of occurrence probabilities adopted by the Japanese Government are likely to be result of interpreting the uncertainties in the data in the most pessimistic way, so as to put emphasis on the need of preparedness against earthquake disasters for the population.

We test a proxy for the time-predictable model that could be applied in information poor settings. We apply a very simple earthquake simulator to the Nankai, Tonankai and Tokai subduction zones that requires only two primary inputs: (1) fault-slip rates, and (2) an estimated magnitude–frequency distribution slope (b-value), which can be defined with 5 parameters. The simulator is intended for use where supporting information like palaeoseismic and historical recurrence data, and fault segmentation observations is absent. However, we use it in a place where all that information is available to assess its potential application for probabilistic forecasting.

We find that the simulator, which imposes no physical geometric rupture barriers (meaning gaps or steps in the faults), can replicate the spatial proportion of fault segment ruptures evident within the Nankai-Tokai zone (within 95 per cent confidence bounds) because of plate convergence rate variability. We calculate a 1–13 per cent 30-yr $M \geq 7.9$ rupture probability for the Tokai segment (E) using simulator earthquake rates and moderate to high coefficients of variation ($\alpha = 0.5\text{--}0.9$). This probability value is lower than, but overlaps values calculated from the characteristic approach (10–19 per cent). Generally, modelled earthquake rate and probability calculations for the Nankai zone more closely match those determined from a characteristic, time-predictable model for segments A–D from $M = 7.9$ to 8.3.

For a region rich in historical accounts and confirmatory tsunami records like the Nankai-Tokai subduction zone of Japan, we believe that detailed earthquake probability calculations that involve interacting faults can be calculated with reasonable certainty, as we have done in the initial sections of this paper. We also calculated earthquake rate and probability results from a simple simulator that assumes a Gutenberg–Richter magnitude–frequency distribution, and found that they are generally comparable. As such, we suggest that these methods might be useful for earthquake forecasting in settings that lack the detailed records available along the Nankai zone.

ACKNOWLEDGMENTS

The authors are grateful to Lynn Sykes and David Jackson for their useful suggestions that contributed to the improvement of the paper.

REFERENCES

- Abercrombie, R.E. & Brune, J.N., 1994. Evidence for a constant b-value above magnitude 0 in the southern San Andreas, San Jacinto and San Miguel fault zones, and at the Long Valley caldera, California, *Geophys. Res. Lett.*, **21**, 1647–1650.
- Ando, M., 1975a. Possibility of a major earthquake in the Tokai district, Japan, and its pre-estimated seismo-tectonic effects, *Tectonophysics*, **27**, 119–140.
- Ando, M., 1975b. Source mechanisms and tectonic significance of historical earthquakes along the Nankai trough, Japan, *Tectonophysics*, **27**, 119–140.
- Aoi, S., Enescu, B., Suzuki, W., Asano, Y., Obara, K., Kunugi, T. & Shiomi, K., 2010. Stress transfer in the Tokai subduction zone from the 2009 Suruga Bay earthquake in Japan, *Nature Geosci.*, **3**, 496–500, doi:10.1038/NGEO885.
- Barka, A.A. & Kandinsky-Cade, K., 1988. Strike-slip fault geometry in Turkey and its influence on earthquake activity, *Tectonics*, **7**, 663–684.
- Console, R. & Catali, F., 2007. A rate-state model for aftershocks triggered by dislocation on a rectangular fault: a review and new insights, *Ann. Geophys.*, **49**(6), 1259–1273.
- Console R., Murru, M., Falcone, G. & Catali, F., 2008. Stress interaction effect on the occurrence probability of characteristic earthquakes in Central Apennines, *J. geophys. Res.*, **113**, B08313, doi:10.1029/2007JB005418.
- Console, R., Murru, M. & Falcone, G., 2010. Perturbation of earthquake probability for interacting faults by static Coulomb stress changes, *J. Seismol.*, **14**, 67–77, doi:10.1007/s10950-008-9149-4.
- ERC, 2001. Report of the Earthquake Research Committee, Subcommittee for long-term evaluation, Headquarters for Earthquake Research Promotion, Japan (in Japanese).
- Furumura, T. & Saito, T., 2009. Integrated ground motion and tsunami simulation for the 1944 Tonankai earthquake using high-performance supercomputers, *J. Disaster Res.*, **4**, 118–126.
- Gutenberg, B. & Richter, C.R., 1954. Magnitude and energy of earthquakes, *Ann. Geophys.*, **9**, 1–15.
- Hagiwara, Y., 1974. Probability of earthquake occurrence as obtained from a Weibull distribution analysis of crustal strain, *Tectonophysics*, **23**, 323–318.
- Hanks, T.C. & Kanamori, H., 1979. A moment magnitude scale, *J. geophys. Res.*, **84**, 2348–2350.
- Harris, R.A., 1992. Peri-collisional extension and the formation of Oman-type ophiolites in the Brooks Range and Banda arc, in *Ophiolites and Their Modern Oceanic Analogues*, Geol. Soc. London Spec. Publ. Vol. 60, pp. 301–325, eds Parsons, L.M., Murton, B.J. & Browning, P., The Geological Society, London.
- Harris, R.A. & Day, S.M., 1993. Dynamics of fault interaction: parallel strike-slip faults, *J. geophys. Res.*, **98**, 4461–4472.
- Harris, R.A. & Day, S.M., 1999. Dynamic 3D simulations of earthquakes on an echelon faults, *Geophys. Res. Lett.*, **26**, 2089–2092.
- Hori, T., Kato, N., Hirahara, K., Baba, T. & Kaneda, Y., 2004. A numerical simulation of earthquake cycles along the Nankai Trough in southwest Japan: lateral variation in frictional property due to the slab geometry controls the nucleation position, *Earth planet. Sci. Lett.*, **228**, 215–226, doi:10.1016/j.epsl.2004.09.033.
- Ishibashi, K., 1976. Re-examination of a great earthquake expected in the Tokai district: possibility of the ‘Suruga bay earthquake’, Abstracts, *Seismol. Soc. Japan*, **2**, 30–34 (in Japanese).
- Ishibashi, K., 1980. Comments on the long-term prediction of the Tokai earthquake, in *Proceedings of the Earthquake Prediction Research Symposium*, National Committee for Seismology in Science Council of Japan and Seismological Society of Japan, pp. 123–125 (in Japanese with English abstract).
- Ishibashi, K., 1981. Specification of a soon-too-occur seismic faulting in the Tokai district, central Japan, based upon seismotectonics, in *Earthquake Prediction—An International Review*, Maurice Ewing Ser. IV, pp. 297–332, eds Simpson, D.W. & Richards, P.G., American Geophysical Union, Washington, DC.
- Ishibashi, K. & Satake, K., 1998. Problems on forecasting great earthquakes in the subduction zones around Japan by means of paleoseismology, *Zisin, J. Seismol. Soc. Japan*, **50**, 1–21 (in Japanese).
- Ishibashi, K., 1999. Great Tokai and Nankai, Japan, earthquakes as revealed by historical seismology: 1. Review of the events until the mid-14th century, Chigaku Zasshi, *J. Geogr.*, **108**, 399–423 (in Japanese with English abstract).
- Ishimoto, M. & Iida, K., 1939. Observations sur les seismes enregistres par le microseimographe construit dernièrement, *Bull. Earthq. Res. Inst. Univ. Tokyo*, **17**, 443–478 (in Japanese with French abstract).

- Ito, T. & Hashimoto, M., 2004. Spatiotemporal distribution of interplate coupling in southwest Japan from inversion of geodetic data, *J. geophys. Res.*, **109**, B02315, doi:10.1029/2002JB002358.
- Jackson, D.D. & Kagan, Y.Y., 1993. Reply to Nishenko and Sykes, *J. geophys. Res.*, **98**, 9917–9920.
- Kagan, Y.Y., 2002a. Seismic moment distribution revisited: statistical results, *Geophys. J. Int.*, **148**, 520–541.
- Kagan, Y.Y., 2002b. Seismic moment distribution revisited: II. Moment conservation principle, *Geophys. J. Int.*, **149**, 731–754.
- Kagan, Y.Y. & Knopoff, L., 1987. Random stress and earthquake statistics: time dependence, *Geophys. J. R. astr. Soc.*, **88**, 723–731.
- Kagan, Y.Y. & Jackson, D.D., 1991. Seismic gap hypothesis: ten years after, *J. geophys. Res.*, **96**(B13), doi:10.1029/91JB02210.
- Kagan, Y.Y. & Jackson, D.D., 1995. New seismic gap hypothesis: five years after, *J. geophys. Res.*, **100**, 3943–3960.
- Lettis, W., Bachhuber, J., Witter, R., Brankman, C., Randolph, C.E., Barka, A., Page, W.D. & Kaya, A., 2002. Influence of releasing step-overs on surface fault rupture and fault segmentation: examples from the 17 August 1999 Izmit earthquake on the North Anatolian fault, Turkey, *Bull. seism. Soc. Am.*, **92**, 19–42.
- López-Ruiz, R., Vázquez-Prada, M., Gómez, J.B. & Pacheco, A.F., 2004. A model of characteristic earthquakes and its implications for regional seismicity, *TerraNova*, **16**, 116–120, doi:10.1111/j.1365-3121.2004.00538.x.
- Marzocchi, W. & Lombardi, A.M., 2008. A double branching model for earthquake occurrence, *J. geophys. Res.*, **113**, B08317, doi:10.1029/2007JB005472.
- Matthews, M.V., Ellsworth, W.L. & Reasenber, P.A., 2002. A Brownian Model for recurrent earthquakes, *Bull. seism. Soc. Am.*, **92**, 2233–2250.
- Mazzotti, S., Le Pichon, X. & Henry, P., 2000. Full interseismic locking of the Nankai and Japan-west Kurile subduction zones: an analysis of uniform elastic strain accumulation in Japan constrained by permanent GPS, *J. geophys. Res.*, **105**, 13 159–13 177.
- McCann, W.R., Nishenko, S.P., Sykes, L.R. & Krause, J., 1979. Seismic gaps and plate tectonics: seismic potential for major boundaries, *Pure appl. Geophys.*, **117**, 1082–1147.
- Mitsui, N. & Hirahara, K., 2004. Simple spring-mass model simulation of earthquake cycle along the Nankai trough in Southwest Japan, *Pure appl. Geophys.*, **161**, 2433–2450, doi:10.1007/s00024-004-2574-6.
- Mochizuki, K. & Obana, K., 2003. Seismic activities along the Nankai trough, *Bull. Earthq. Res. Inst.*, **78**, 185–195.
- Mogi, K., 1968. Sequential occurrences of recent great earthquakes, *J. Phys. Earth*, **16**, 30–60.
- Mogi, K., 1986. Strain accumulation and rupture processes in the subduction zone along the Nankai-Suruga trough in western Japan, *Am. Geophys. Monogr.*, **37**, 183–194.
- Mogi, K., 2004. Two grave issues concerning the expected Tokai earthquake, *Earth Planets Space*, **56**(li), lxvi.
- Nishenko, S.P., 1991. Circum-Pacific seismic potential 1989–1999, *Pure appl. Geophys.*, **135**, 169–259.
- Nishenko, S.P. & Buland, R., 1987. A generic recurrence interval distribution for earthquake forecasting, *Bull. seism. Soc. Am.*, **77**, 1382–1399.
- Nishenko, S.P. & Sykes, L.R., 1993. Comment on ‘Seismic gap hypothesis: ten years after’ by Y.Y. Kagan and D.D. Jackson, *J. geophys. Res.*, **98**, 9909–9916.
- Nishimura, T., Munekane, H. & Yarai, H., 2011. The 2011 off the Pacific coast of Tohoku earthquake and its aftershocks observed by GEONET, *Earth Planets Space*, **63**, 631–636.
- Page, M., 2010. Reply to Schwartz and Open Discussion, *Seismol. Res. Lett.*, **81**, 331.
- Parsons, T., 2008. Monte Carlo method for determining earthquake recurrence parameters from short paleoseismic catalogs: example calculations for California, *J. geophys. Res.*, **113**, doi:10.1029/2007JB004998.
- Parsons, T. & Geist, E.L., 2009. Is there basis for preferring characteristic earthquakes over Gutenberg-Richter distributions on individual faults in probabilistic earthquake forecasting?, *Bull. seism. Soc. Am.*, **99**, 2012–2019, doi:10.1785/0120080069.
- Reid, H.F., 1910. The Mechanics of the Earthquake, *The California Earthquake of April 18, 1906*, Report of the State Earthquake Investigation Commission, Vol. 2, Carnegie Institution of Washington Publication 87, Washington, DC.
- Rikitake, T., 1975. Statistics of ultimate strain of the earth’s crust and probability of earthquake occurrence, *Tectonophysics*, **26**, 1–21.
- Rikitake, T., 1976. Recurrence of great earthquakes at subduction zones, *Tectonophysics*, **35**, 335–362.
- Rikitake, T., 1977. Probability of a great earthquake to recur off the Pacific coast of Central Japan, *Tectonophysics*, **42**, T43–T51.
- Rong, Y., Jackson, D.D. & Kagan, Y.Y., 2003. Seismic gaps and earthquakes, *J. geophys. Res.*, **108**(B10), 2471, doi:10.1029/2002JB002334.
- Sagiya, T. & Thatcher, W., 1999. Coseismic slip resolution along a plate boundary megathrust: the Nankai Trough, southwest Japan, *J. geophys. Res.*, **104**, 1111–1129.
- Sangawa, A., 1999. Earthquake traces carved in excavations in the past 2,000 years, *Chkyu Monthly*, **24**, 56–63 (in Japanese).
- Sangawa, A., 2011. What large earthquakes have Japanese people experienced?, in *Introduction to Earthquake Archeology*, Heibonsha, Tokyo 259pp. (in Japanese).
- Sato, R., Abe, K., Okada, Y., Shimazaki, K. & Suzuki, H., 1989. *Handbook of Earthquake Fault Parameters in Japan*, Kashima, Tokyo, 390pp. (in Japanese).
- Schorlemmer, D., Neri, G., Weimer, S. & Mostaccio, A., 2003. Stability and significance tests for b-value anomalies: example from the Tyrrhenian Sea, *Geophys. Res. Lett.*, **30**, doi:10.1029/2003GL017335.
- Schorlemmer, D., Weimer, S. & Wyss, M., 2004. Earthquake statistics at Parkfield: 1. Stationarity of b values, *J. geophys. Res.*, **109**, doi:10.1029/2004JB003234.
- Schwartz, D.P., 2010. Do large earthquakes on faults follow a Gutenberg-Richter or characteristic distribution?: a characteristic view, *Seismol. Res. Lett.*, **81**, 331.
- Schwartz, D.P. & Coppersmith, K.J., 1984. Fault behavior and characteristic earthquakes: examples from the Wasatch and San Andreas fault zones, *J. geophys. Res.*, **89**, 5681–5698.
- Shimazaki, K. & Nakata, T., 1980. Seismic gap hypothesis: ten years later, *Geophys. Res. Lett.*, **7**, 279–282.
- Stein, R., Barka, A. & Dieterich, J., 1997. Progressive failure on the North Anatolian fault since 1939 by earthquake stress triggering, *Geophys. J. Int.*, **128**, 594–604.
- Stein, S. & Newman, A., 2004. Characteristic and uncharacteristic earthquakes as possible artifacts: applications to the New Madrid and Wabash seismic zones, *Seimol. Res. Lett.*, **75**, 173–187.
- Stein, S., Friedrich, A. & Newman, A., 2005. Dependence of possible characteristic earthquakes on spatial sampling: illustration for the Wasatch seismic zone, Utah, *Seismol. Res. Lett.*, **76**, 432–436.
- Sykes, L.R. & Menke, W., 2006. Repeat times of large earthquakes: implications for earthquake mechanics and long-term prediction, *Bull. seism. Soc. Am.*, **96**(5), 1569–1596, doi:10.1785/0120050083.
- Toda, S., Lin, J. & Stein, R., 2011. Using the 2011 M = 9.0 Tohoku earthquake to test the Coulomb stress triggering hypothesis and to calculate faults brought closer to failure, submitted to Tohoku Earthquake, *Earth Planets Space*, **63**, 725–730.
- Utsu, T., 1977. Possibility of a great earthquake in the Tokai district, central Japan, *J. Phys. Earth*, **25**, S219–S230.
- Wang, K., Wada, I. & Ishikawa, Y., 2004. Stresses in the subducting slab beneath southwest Japan and relation with plate geometry, tectonic forces, slab dehydration, and damaging earthquakes, *J. geophys. Res.*, **109**, doi:10.1029/2003JB002888.
- Wells, D.L. & Coppersmith, K.J., 1994. New empirical relationships among magnitude, rupture length, rupture width, rupture area, and surface displacement, *Bull. seism. Soc. Am.*, **84**, 974–1002.
- Wesnousky, S.G., 1994. The Gutenberg-Richter or characteristic earthquake distribution, which is it?, *Bull. seism. Soc. Am.*, **84**, 1940–1959.
- Westerhaus, M., Wyss, M., Yilmaz, R. & Zschau, J., 2002. Correlating variations of b values and crustal deformation during the 1990’s may have pinpointed the rupture initiation of the Mw = 7.4 Izmit earthquake of 1999 August 17, *Geophys. J. Int.*, **148**, 139–152.

Working Group on California Earthquake Probabilities (WGCEP), 1995. Seismic hazards in Southern California: probable earthquakes, 1994 to 2024, *Bull. seism. Soc. Am.*, **85**, 379–439.

Working Group on California Earthquake Probabilities (WGCEP), 2003. Earthquake probabilities in the San Francisco Bay region: 2002 to 2031. Open-File Rep, U.S. Geol. Surv., 03–214.

Working Group on California Earthquake Probabilities (WGCEP), 2008. The uniform California earthquake rupture forecast, version 2 (UCERF 2). Open-File Rep, U.S. Geol. Surv., 07–1437.

Wyss, M., Sammis, C.G., Nadeau, R.M. & Weimer, S., 2004. Fractal dimension and b-value on creeping and locked patches of the San Andreas fault near Parkfield, California, *Bull. seism. Soc. Am.*, **94**, 410–421.